

# Partitioned Finite Element Method for Power-Preserving Structural Discretization with Mixed-Boundary Conditions<sup>\*</sup>

Andrea Brugnoli<sup>\*</sup> Flávio Luiz Cardoso-Ribeiro<sup>\*\*</sup>  
Ghislain Haine<sup>\*</sup> Paul Kotyczka<sup>\*\*\*</sup>

<sup>\*</sup> ISAE-SUPAERO, Université de Toulouse, 10 Avenue Edouard Belin,  
BP-54032, 31055 Toulouse Cedex 4, France (e-mail: {andrea.brugnoli,  
ghislain.haine}@isae.fr).

<sup>\*\*</sup> Instituto Tecnológico de Aeronáutica, Brazil  
(e-mail: flaviocr@ita.br).

<sup>\*\*\*</sup> Institute of Automatic control, Technische Universität München,  
85748 Garching, Germany (e-mail: kotyczka@tum.de).

---

**Abstract:** The propagation of acoustic waves in a 2D geometrical domain under **mixed boundary** control is here described by means of the **port Hamiltonian** (pH) formalism. A finite element based method is employed to obtain a consistent discretized model. To construct a model with **mixed boundary** control two different methodology are detailed: one employs Lagrange multipliers, the other relies on a virtual domain decomposition to interconnect models with different **causality**. The two approaches are assessed numerically, by comparing the Hamiltonian trend for progressively refined meshes.

Keywords: Aeroacoustics, port-Hamiltonian systems (pHs), Partitioned Finite Element Method (PFEM), mixed boundary control.

---

## 1. INTRODUCTION

The port-Hamiltonian (pH) formalism has **demonstrate** to be valuable modelling paradigm, capable of highlighting important properties of dynamical **system** (Duindam et al. [2009]) and representing a huge class of **system**, either finite- **either infinite dimensional** (van der Schaft and Maschke [2002]). Obtaining **finite dimensional** representations that preserve the proprieties of the continuous system at a discrete level is not a trivial task. Many techniques (e.g. Moulla et al. [2012]) **cannot treat higher geometrical dimensions**. Finite differences Trenchant et al. [2018] can be used for 2D problems but the actual implementation cannot be automated easily. A finite element approach dealing with different boundary causality has been proposed in Kotyczka [2016] but the mesh construction depends on some degrees of freedom and finding the right combination is not straightforward.

The method of choice for this paper is detailed in Cardoso-Ribeiro et al. [2019]. It represents the extension of the mixed finite element method (Gatica [2014]) to pH systems and as such it can be easily implemented using standard finite elements library (e.g. Rathgeber et al. [2017]). Because of the possibility of selecting the natural boundary

condition that appear in the **discretization** this method is referred to as partitioned finite element method (PFEM). Despite the many advantages of PFEM, the inclusion of mixed causality demands additional care. A detailed discussion, both at a theoretical and numerical level, on mixed boundary control problems in 2D geometric domains may be found in Grisvard [2011].

In this **work** to illustrate how mixed boundary control are handled in PFEM the propagation of acoustic waves in a cylindrical duct is considered. As a Dirichlet control an impedance boundary control is taken over the lateral surface of the cylinder. On the remaining boundary a constant flux is taken at the inlet and outlet. Two different **methodology** to treat the **mixed boundary** causalities are detailed and numerically compared.

In Section 2 the problem under consideration is detailed. The **boundary and initial boundary conditions** are assumed to be axis-symmetric. This allows reducing the problem from a 3D to a 2D geometry. In Section 3 the partitioned finite element method is recalled, under the hypothesis of uniform boundary conditions. In Section 4 the treatment of mixed boundary conditions is described. One strategy rely on the usage of Lagrange multipliers to enforce the Dirichlet boundary condition. The other requires the constructions of two models with different causality by splitting the domain into two parts. These two models are then interconnected to get a final system with **mixed boundary** inputs. In Sections 5 the numerical

---

<sup>\*</sup> This work is supported by the project ANR-16-CE92-0028, entitled *Interconnected Infinite-Dimensional systems for Heterogeneous Media*, INFIDHEM, financed by the French National Research Agency (ANR) and the Deutsche Forschungsgemeinschaft (DFG). Further information is available at <https://websites.isae-supaero.fr/infidhem/the-project>.

simulations provided by the two different methods are presented. By progressively refining the mesh size, it is shown that, for both methods, the Hamiltonian converges to the one given by a reference solution.

## 2. PROBLEM STATEMENT: MODEL DESCRIPTION

In this section we state the problem under consideration by making use of a port-Hamiltonian model. The reader can consult Jacob and Zwart [2012] for a comprehensive introduction and links towards classical PDE models.

The propagation of sound in air inside is modeled by Trenchant et al. [2018]

$$\frac{\partial}{\partial t} \begin{bmatrix} \chi_s p \\ \mu_0 \mathbf{v} \end{bmatrix} = - \begin{bmatrix} 0 & \text{div} \\ \text{grad} & 0 \end{bmatrix} \begin{bmatrix} p \\ \mathbf{v} \end{bmatrix}, \quad (1)$$

on  $\Omega \subset \mathbb{R}^3$ .  $p \in \mathbb{R}$  and  $\mathbf{v} \in \mathbb{R}^3$  denote the variations of pressure and velocity from a steady state,  $\mu_0$  is the steady state mass density, and  $\chi_s$  represents a constant adiabatic compressibility factor. A cylindrical duct of length  $L$  and radius  $R$  is considered as physical domain ( $\Omega = \{x \in [0, L], r \in [0, R], \theta \in [0, 2\pi]\}$ ). Denoting by  $x, r, \theta$  the axial, radial and tangential coordinate, the following boundary conditions are imposed

$$p(x, R, \theta) = -\mathcal{Z}(x, t) v_r(x, R, \theta), \quad (2)$$

$$\mathbf{v} \cdot \mathbf{n}(0, r, \theta) = -v_x(0, r, \theta) = -f(r), \quad (3)$$

$$\mathbf{v} \cdot \mathbf{n}(L, r, \theta) = +v_x(L, r, \theta) = +f(r). \quad (4)$$

As the main focus is the treatment of mixed boundary conditions, it is assumed that the impedance operator  $\mathcal{Z}$  is non invertible. For the initial boundary conditions, it is assumed

$$\begin{aligned} p^0(x, r, \theta) &= 0, \\ v_x^0(x, r, \theta) &= f(r), \\ v_r^0(x, r, \theta) &= g(r), \\ v_\theta^0(x, r, \theta) &= 0. \end{aligned} \quad (5)$$

This model describes the behavior of an axis-symmetrical flow subjected to an impedance condition on the lateral surface. Because of symmetry the model can be reduced to a 2D problem in polar coordinates over the domain  $\Omega_r = \{x \in [0, L], r \in [0, R]\}$ . The reduced system reads

$$\frac{\partial}{\partial t} \begin{bmatrix} \chi_s p \\ \mu_0 v_x \\ \mu_0 v_r \end{bmatrix} = - \begin{bmatrix} 0 & \partial_x & \partial_r + 1/r \\ \partial_x & 0 & 0 \\ \partial_r & 0 & 0 \end{bmatrix} \begin{bmatrix} p \\ v_x \\ v_r \end{bmatrix}. \quad (6)$$

The boundary conditions must now account for the symmetry condition at  $r = 0$ , leading to the additional condition  $\mathbf{v} \cdot \mathbf{n}(x, 0) = v_r(x, 0) = 0$ . System (6) can be rewritten compactly as a pH system in co-energy variables

$$\mathcal{Q}^{-1} \partial_t e = \mathcal{J} e \quad (7)$$

where  $\mathcal{Q}^{-1} = \text{diag}([\chi_s, \mu_0, \mu_0])$  is a bounded, coercive operator and  $e = [p, v_x, v_r]$  is the vector of the co-energy variables. The interconnection operator  $\mathcal{J}$  can be decomposed in the sum of  $\mathcal{J} = \mathcal{J}_{\text{div}} + \mathcal{J}_{\text{grad}}$

$$\mathcal{J}_{\text{div}} = - \begin{bmatrix} 0 & \partial_x & \partial_r + 1/r \\ 0 & 0 & 0 \\ 0 & 0 & 0 \end{bmatrix}, \quad \mathcal{J}_{\text{grad}} = - \begin{bmatrix} 0 & 0 & 0 \\ \partial_x & 0 & 0 \\ \partial_r & 0 & 0 \end{bmatrix}. \quad (8)$$

Such a decomposition is meaningful as  $\mathcal{J}_{\text{grad}}^* = -\mathcal{J}_{\text{div}}$ , where  $*$  denote the formal adjoint operator and it is especially useful to illustrate the partitioned finite element method

## 3. RECALL ON THE PARTITIONED FINITE ELEMENT METHOD

In this section the partitioned finite element method Cardoso-Ribeiro et al. [2019] is recalled by considering uniform (either Neumann, either Dirichlet in standard terminology) boundary conditions. The idea boils down to three simple steps:

- (1) write the system in weak form;
- (2) perform integration by parts to get the chosen boundary control;
- (3) select the finite element spaces to achieve a finite-dimensional system.

The second step is crucial as it determines which boundary condition appear as input, defining the causality of the system.

In order to perform the first step, consider the standard  $L^2$  inner product in polar coordinates

$$(f, g)_{\Omega_r} = \int_{\Omega_r} f \cdot g \, r \, dr \, dx = \int_{\Omega_r} f \cdot g \, d\Omega_r.$$

The weak form is obtained by considering the scalar product of system (7) against a test function  $w = [w_p, w_{vx}, w_{vy}] = [w_p, \mathbf{w}_v]$

$$(w, \mathcal{Q}^{-1} \partial_t e)_{\Omega_r} = (w, \mathcal{J} e)_{\Omega_r}. \quad (9)$$

As  $\mathcal{Q}$  is coercive the inner product on the left hand side corresponds to a symmetric and coercive bilinear form  $m(w, \partial_t e) := (w, \mathcal{Q}^{-1} \partial_t e)_{\Omega_r}$ . The integration by parts will define which boundary control will appear explicitly.

### 3.1 Neumann boundary control

If the integration by parts is applied on  $\mathcal{J}_{\text{div}}$  then the right hand-side of Eq. (9) becomes

$$(w, \mathcal{J} e)_{\Omega_r} = (v, \mathcal{J}_{\text{grad}} e)_{\Omega_r} - (\mathcal{J}_{\text{grad}} w, e)_{\Omega_r} + (w_p, u_N)_{\partial\Omega_r}.$$

The skew-symmetric bilinear form

$$j_{\text{grad}}(w, e) := (w, \mathcal{J}_{\text{grad}} e)_{\Omega_r} - (\mathcal{J}_{\text{grad}} w, e)_{\Omega_r}$$

may now be introduced, together with the boundary form

$$(w_p, u_N)_{\partial\Omega_r} = \int_{\partial\Omega_r} w_p u_N \, d\Gamma_r, \quad (10)$$

where  $u_N = \mathbf{v} \cdot \mathbf{n}|_{\partial\Omega}$  and  $d\Gamma_r = r \, ds$  is the infinitesimal surface. The corresponding output  $y_N = p|_{\partial\Omega}$ . The system in weak form under Neumann boundary control is then written as

$$\begin{aligned} m(w, \partial_t e) &= j_{\text{grad}}(w, e) + (w_p, u_N)_{\partial\Omega_r}, \\ (w_N, y_N)_{\partial\Omega_r} &= (w_N, p)_{\partial\Omega_r} \end{aligned} \quad (11)$$

### 3.2 Dirichlet boundary control

If the in-integration by parts is carried out on  $\mathcal{J}_{\text{grad}}$  then the right hand-side of (9) becomes

$$(w, \mathcal{J} e)_{\Omega_r} = (v, \mathcal{J}_{\text{div}} e)_{\Omega_r} - (\mathcal{J}_{\text{div}} w, e)_{\Omega_r} + (\mathbf{w}_v \cdot \mathbf{n}, u_D)_{\partial\Omega_r}.$$

The skew-symmetric bilinear form

$$j_{\text{div}}(w, e) := (w, \mathcal{J}_{\text{div}} e)_{\Omega_r} - (\mathcal{J}_{\text{div}} w, e)_{\Omega_r}$$

is introduced, together with the boundary form

$$(\mathbf{w}_v \cdot \mathbf{n}, u_D)_{\partial\Omega_r} = \int_{\partial\Omega_r} \mathbf{w}_v \cdot \mathbf{n} u_D \, d\Gamma_r, \quad (12)$$

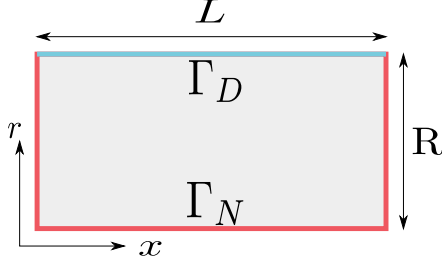


Fig. 1. Boundary partition for the problem.

where  $u_D = p|_{\partial\Omega}$ . Adding the conjugated output  $y = \mathbf{v} \cdot \mathbf{n}|_{\partial\Omega}$ , the system in weak form under Dirichlet boundary control is then written as

$$\begin{aligned} m(w, \partial_t e) &= j_{\text{div}}(w, e) + (\mathbf{w}_v \cdot \mathbf{n}, u_D)_{\partial\Omega_r}, \\ (w_D, y_D)_{\partial\Omega_r} &= (w_D, \mathbf{v} \cdot \mathbf{n})_{\partial\Omega_r} \end{aligned} \quad (13)$$

#### 4. EXTENSION FOR MIXED-BOUNDARY CONDITIONS

In this section we consider the case in which Neumann and Dirichlet boundary control co-exist. The partitioned finite element method allow to treat this case by means of two different approach. One relies on a differential-algebraic formulation, the other on a purely differential formulation by exploiting a classical interconnection of pH system together with a domain decomposition.

##### 4.1 Lagrange Multipliers

This approach can equivalently use Eq. (11) or Eq. (13) as a starting point. The weak form (11) will be used both for the illustration of the method and for numerical computations. The boundary is split in two partition (see Fig. 1). For the time being generic inputs  $u_D, u_N$  for the Dirichlet and Neumann conditions are considered. First of all the boundary term in Eq. (10) needs to be revisited. The quantity  $\mathbf{v} \cdot \mathbf{n}|_{\partial\Omega_r}$  is known on  $\Gamma_N$ , while on  $\Gamma_D$  it corresponds to the Lagrange multiplier  $\lambda_D$  needed to enforce the Dirichlet boundary condition

$$\int_{\partial\Omega_r} w_p \mathbf{v} \cdot \mathbf{n} d\Gamma_r = \int_{\Gamma_N} w_p u_N d\Gamma_r + \int_{\Gamma_D} w_p \lambda_D d\Gamma_r. \quad (14)$$

The constraint is enforced by weakly imposing a generic in-homogeneous Dirichlet condition

$$\int_{\Gamma_D} w_\lambda (p - u_D) d\Gamma_r = 0. \quad (15)$$

The system in weak form is obtained by using Eqs. (11), (10), (14) and (15):

$$\begin{aligned} m(w, \partial_t e) &= j_{\text{grad}}(w, e) + (w_p, u_N)_{\Gamma_N} + (w_p, \lambda_D)_{\Gamma_D}, \\ 0 &= -(w_\lambda, p)_{\Gamma_D} + (w_\lambda, u_D)_{\Gamma_D}, \\ (w_N, y_N)_{\Gamma_N} &= (w_N, p)_{\Gamma_N}, \\ (w_D, y_D)_{\Gamma_D} &= (w_D, \lambda_D)_{\Gamma_D}. \end{aligned} \quad (16)$$

A Galerkin method can now be applied to retrieve a finite dimensional pH system. Corresponding test and trial functions  $([w_p, p], [\mathbf{w}_v, \mathbf{v}], [w_N, u_N, y_N])$  and  $([w_\lambda, \lambda_D, w_D, u_D, y_D])$  are discretized using the same basis, leading to the finite dimensional pHDAE (Beattie et al. [2018]):

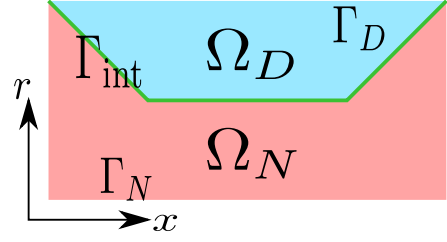


Fig. 2. Virtual decomposition of the domain.

$$\begin{aligned} \begin{bmatrix} \mathbf{M} & \mathbf{0} \\ \mathbf{0} & \mathbf{0} \end{bmatrix} \frac{d}{dt} \begin{bmatrix} \mathbf{e} \\ \boldsymbol{\lambda}_D \end{bmatrix} &= \begin{bmatrix} \mathbf{J} & \mathbf{G}_D \\ -\mathbf{G}_D^T & \mathbf{0} \end{bmatrix} \begin{bmatrix} \mathbf{e} \\ \boldsymbol{\lambda}_D \end{bmatrix} + \begin{bmatrix} \mathbf{B}_N & \mathbf{0} \\ \mathbf{0} & \mathbf{B}_D \end{bmatrix} \begin{bmatrix} \mathbf{u}_N \\ \mathbf{u}_D \end{bmatrix}, \\ \begin{bmatrix} \mathbf{y}_N \\ \mathbf{y}_D \end{bmatrix} &= \begin{bmatrix} \mathbf{B}_N^T & \mathbf{0} \\ \mathbf{0} & \mathbf{B}_D^T \end{bmatrix} \begin{bmatrix} \mathbf{e} \\ \boldsymbol{\lambda}_D \end{bmatrix}. \end{aligned} \quad (17)$$

*Remark 1.* The output has been defined incorporating the mass matrix. The actual degrees of freedom corresponding to the output are found by solving

$$\begin{bmatrix} \mathbf{M}_{\Gamma_N} & \mathbf{0} \\ \mathbf{0} & \mathbf{M}_{\Gamma_D} \end{bmatrix} \begin{bmatrix} \hat{\mathbf{y}}_N \\ \hat{\mathbf{y}}_D \end{bmatrix} = \begin{bmatrix} \mathbf{y}_N \\ \mathbf{y}_D \end{bmatrix}, \quad \mathbf{M}_{\partial\Omega} \hat{\mathbf{y}} = \mathbf{y}. \quad (18)$$

Concerning the actual boundary conditions, on  $\Gamma_D$  the impedance condition (2) is applied while on  $\Gamma_N$  the inlet and outlet flow condition (3), (4) hold on the left and right side of the rectangle. The impedance is imposed by applying the feedback law

$$\mathbf{u}_D = -\mathbf{Z} \mathbf{y}_D.$$

The impedance, assuming that  $\mathbf{u}_D$  has dimension  $m$ , matrix is simply given by

$$\mathbf{Z} = \text{diag}([\mathcal{Z}(x_{u_1^m}, t), \dots, \mathcal{Z}(x_{u_D^m}, t)]).$$

The Neumann boundary condition is imposed by projection on the  $u_N$  space. The boundary controlled system becomes

$$\begin{bmatrix} \mathbf{M} & \mathbf{0} \\ \mathbf{0} & \mathbf{0} \end{bmatrix} \frac{d}{dt} \begin{bmatrix} \mathbf{e} \\ \boldsymbol{\lambda}_D \end{bmatrix} = \begin{bmatrix} \mathbf{J} & \mathbf{G}_D \\ -\mathbf{G}_D^T & -\mathbf{R} \end{bmatrix} \begin{bmatrix} \mathbf{e} \\ \boldsymbol{\lambda}_D \end{bmatrix} + \begin{bmatrix} \mathbf{b}_N \\ \mathbf{0} \end{bmatrix}, \quad (19)$$

with  $\mathbf{R} = \mathbf{B}_D \mathbf{Z} \mathbf{B}_D^T$  a symmetric positive definite matrix.

*Remark 2.* The actual boundary conditions can be imposed directly in the weak formulation considering that  $\mathbf{u}_D = -\mathbf{Z} \mathbf{v} \cdot \mathbf{n} = -\mathbf{Z} \boldsymbol{\lambda}_D$ . Consequently, the computation of the dissipation matrix  $\mathbf{R}$  modifies as it relies on (15). This amounts to applying to system (19) the control law

$$\mathbf{u}_D = -\mathbf{M}_{D,\mathcal{Z}}^{-1} \mathbf{M}_{D,\mathcal{Z}} \mathbf{M}_{D,\mathcal{Z}}^{-1} \mathbf{y}_D = -\hat{\mathbf{Z}} \mathbf{y}_D,$$

where  $\mathbf{M}_{D,\mathcal{Z}}$  corresponds to the mass matrix associated to the weighted inner product  $(w_D, \mathcal{Z} y_D)_{\Gamma_D}$ .

##### 4.2 Virtual Domain Decomposition

In order to apply this methodology the domain has to be split into two domains. The shared boundary connecting the two can be freely chosen. For the given geometry, the separation line that allows the generation of more regular meshes is a trapezoidal one given in Fig. 2. Starting from the PDE (7) two weak formulations are constructed: one integrating over  $\Omega_D$ , the other over  $\Omega_N$ :

$$(w, \mathcal{Q}^{-1} \partial_t e)_{\Omega_N} = (w, \mathcal{J} e)_{\Omega_N}, \quad (20)$$

$$(w, \mathcal{Q}^{-1} \partial_t e)_{\Omega_N} = (w, \mathcal{J} e)_{\Omega_D}, \quad (21)$$

Then, Eqs. (20), (21) are manipulated according to §3.1, §3.2, respectively:

$$\begin{aligned} m^{\Omega_N}(w, \partial_t e) &= j_{\text{grad}}^{\Omega_N}(w, e) + (w_p, u_N)_{\partial\Omega_N}, \\ m^{\Omega_D}(w, \partial_t e) &= j_{\text{div}}^{\Omega_D}(w, e) + (\mathbf{w}_v \cdot \mathbf{n}, u_D)_{\partial\Omega_D}, \end{aligned} \quad (22)$$

where the superscript  $\Omega_{N,D}$  denote that the bilinear forms are obtained by integration on each sub-domain. The boundary terms in (22) are then split into two **contribution**  $\partial\Omega_N = \Gamma_N \cup \Gamma_{\text{int}}$ ,  $\partial\Omega_D = \Gamma_D \cup \Gamma_{\text{int}}$  so that the common boundary is highlighted

$$\begin{aligned} (w_p, u_N)_{\partial\Omega_N} &= (w_p, u_N)_{\Gamma_N} + (w_p, u_N^{\text{int}})_{\Gamma_{\text{int}}}, \\ (\mathbf{w}_v \cdot \mathbf{n}, u_D)_{\partial\Omega_D} &= (\mathbf{w}_v \cdot \mathbf{n}, u_D)_{\Gamma_D} + (\mathbf{w}_v \cdot \mathbf{n}, u_D^{\text{int}})_{\Gamma_{\text{int}}}. \end{aligned}$$

Applying a Galerkin method to system (22) leads to two finite dimensional pH systems

$$\begin{aligned} \mathbf{M}_N \frac{de_N}{dt} &= \mathbf{J}_N e_N + \mathbf{B}_{N,\text{int}} \mathbf{u}_N^{\text{int}} + \mathbf{B}_N \mathbf{u}_N, \\ \mathbf{y}_N^{\text{int}} &= \mathbf{M}_{\Gamma_{\text{int}}} \hat{\mathbf{y}}_N^{\text{int}} = \mathbf{B}_{N,\text{int}}^T e_N, \\ \mathbf{y}_N &= \mathbf{M}_{\Gamma_N} \hat{\mathbf{y}}_N = \mathbf{B}_N^T e_N, \end{aligned} \quad (23)$$

and

$$\begin{aligned} \mathbf{M}_D \frac{de_D}{dt} &= \mathbf{J}_D e_D + \mathbf{B}_{D,\text{int}} \mathbf{u}_D^{\text{int}} + \mathbf{B}_D \mathbf{u}_D, \\ \mathbf{y}_D^{\text{int}} &= \mathbf{M}_{\Gamma_{\text{int}}} \hat{\mathbf{y}}_D^{\text{int}} = \mathbf{B}_{D,\text{int}}^T e_D, \\ \mathbf{y}_D &= \mathbf{M}_{\Gamma_D} \hat{\mathbf{y}}_D = \mathbf{B}_D^T e_D. \end{aligned} \quad (24)$$

In order to get a final dimensional system with mixed causality, systems (23), (24) have to be **interconnecting** using a classical gyrator interconnection. Considering that the pressure field is continuous at  $\Gamma_{\text{int}}$ , ~~that for~~ the outward normal ~~it holds~~  $\mathbf{n}_D|_{\Gamma_{\text{int}}} = -\mathbf{n}_N|_{\Gamma_{\text{int}}}$  and that corresponding degrees of freedom have to be matched, the correct interconnection reads

$$\begin{aligned} \mathbf{u}_N^{\text{int}} &= -\hat{\mathbf{y}}_D^{\text{int}} = -\mathbf{M}_{\Gamma_{\text{int}}}^{-1} \mathbf{y}_D^{\text{int}}, \\ \mathbf{u}_D^{\text{int}} &= \hat{\mathbf{y}}_N^{\text{int}} = \mathbf{M}_{\Gamma_{\text{int}}}^{-1} \mathbf{y}_N^{\text{int}}. \end{aligned} \quad (25)$$

This interconnection establishes that the power is exchanged without loss between the two systems

$$\mathbf{u}_D^{\text{int}} \cdot \mathbf{y}_D^{\text{int}} + \mathbf{u}_N^{\text{int}} \cdot \mathbf{y}_N^{\text{int}} = 0. \quad (26)$$

The resulting interconnected system is written as

$$\begin{aligned} \mathbf{M}_{ND} \frac{de_{ND}}{dt} &= \mathbf{J}_{ND} e_{ND} + \mathbf{B}_{ND} \mathbf{u}_{ND}, \\ \mathbf{y}_{ND} &= \mathbf{B}_{ND}^T e_{ND}. \end{aligned} \quad (27)$$

The interconnection matrix exhibits a coupling between the two subdomains

$$\mathbf{J}_{ND} = \begin{bmatrix} \mathbf{J}_N & -\mathbf{C} \\ \mathbf{C}^T & \mathbf{J}_D \end{bmatrix},$$

where  $\mathbf{C} = \mathbf{B}_{N,\text{int}} \mathbf{M}_{\Gamma_{\text{int}}}^{-1} \mathbf{B}_{D,\text{int}}^T$ . The other matrices and vectors are simply given **concatenation** of each **subdomain** part

$$\begin{aligned} \mathbf{M}_{ND} &= \text{diag}(\mathbf{M}_N, \mathbf{M}_D), & \mathbf{B}_{ND} &= \text{diag}(\mathbf{B}_N, \mathbf{B}_D), \\ \mathbf{e}_{ND} &= [\mathbf{e}_N, \mathbf{e}_D], & \mathbf{u}_{ND} &= [\mathbf{u}_N, \mathbf{u}_D]. \end{aligned}$$

Now that a model with different causality has been obtained, the actual boundary **condition can** be plugged into the system as it was done in §4.1. This leads to the final system

$$\mathbf{M}_{ND} \frac{de_{ND}}{dt} = (\mathbf{J}_{ND} - \mathbf{R}_{ND}) e_{ND} + \mathbf{b}_{ND}, \quad (28)$$

where  $\mathbf{R}_{ND} = \text{diag}(\mathbf{0}, \mathbf{R}_D)$  and  $\mathbf{R}_D = \mathbf{B}_D \mathbf{Z} \mathbf{B}_D^T$ .

Physical Parameters		Simulation Settings	
$L$	2 [m]	ODE Integrator	RK 45
$R$	1 [m]	DAE Integrator	IDA
$\mu_0$	1.225 [kg/m <sup>3</sup> ]	$t_{\text{fin}}$	0.1[s]
$c_0$	340 [m/s]		
$\chi_s$	7.061 [ $\mu\text{Pa}$ ] <sup>-1</sup>		
$v_0$	1 [m/s]		

Table 1. Simulation settings and parameters.

## 5. NUMERICAL RESULTS AND DISCUSSIONS

In this section a numerical illustration of the two methodology is presented. The Hamiltonian trend given by the **differential-algebraic system** and the purely differential are compared with respect to a reference solution. The reference is set to the DAE solution on a very fine mesh.

The acoustic waves in air flow in a duct is considered. The impedance and the axial and radial flows expressions are the following

$$\begin{aligned} \mathcal{Z}(x, t) &= \mathbf{1} \left\{ \frac{1}{3}L \leq x \leq \frac{2}{3}L, t \geq 0.2 t_{\text{fin}} \right\} \mu_0 c_0, \\ f(r) &= \left( 1 - \frac{r^2}{R^2} \right) v_0 \\ g(r) &= 16 \frac{r^2}{R^4} (R - r)^2 v_0 \end{aligned}$$

The initial condition are selected according to (5):

$$\begin{aligned} p^0(x, r) &= 0, \\ v_x^0(x, r) &= f(r), \\ v_r^0(x, r) &= g(r). \end{aligned}$$

A radial component of the velocity allows to highlight the effect of the impedance. The velocity profile satisfy some regularity conditions so that the transition between Neumann and Dirichlet boundary conditions is smooth. In order to get a finite dimensional discretization the fields are approximated using the following finite element families for both approaches:

- $p$  is interpolated using order 1 Lagrange polynomials;
- $\mathbf{v}$  is interpolated using order 2 Raviart-Thomas polynomials;
- the boundary variables  $u_N$  are approximated by Lagrange polynomial of order 1 defined on the boundary  $\Gamma_D$  (for  $\lambda_D, u_D$ ) or  $\Gamma_N$  (for  $u_N$ ).

Such a choice guarantees the conformity with respect to the operator  $\mathcal{J}$ . The matrices are obtained by using Firedrake (Rathgeber et al. [2017]). The reference solution, obtained by using the DAE **approach on a very fine mesh**, is plotted in Fig. 3, where the two contribution to the total energy

$$H_p = \frac{1}{2} \chi_s p^2, \quad H_v = \frac{1}{2} \mu_0 \mathbf{v} \cdot \mathbf{v},$$

are highlighted. The Dirichlet condition induces a continuous transfer from radial kinetic energy into pressure potential. The impedance acts by dissipating the radial component of the velocity so that only the axial flow contribution is left. The total energy at the initial time of the simulation is given only by the kinetic energy

$$H_v^0 = H_{vx}^0 + H_{vr}^0 = \frac{1}{2} \int_0^L \int_0^R \mu_0 [(v_x^0)^2 + (v_r^0)^2] r dr dx.$$

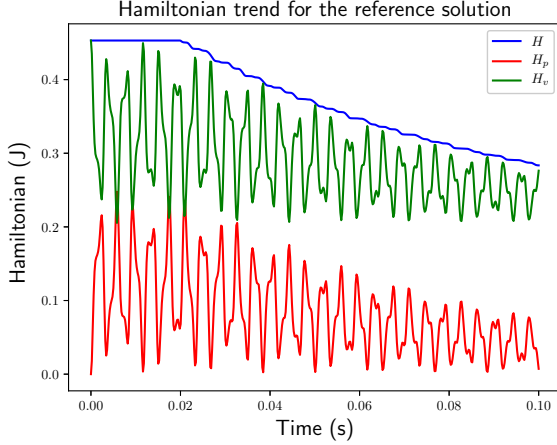


Fig. 3. Hamiltonian trend for reference solution.

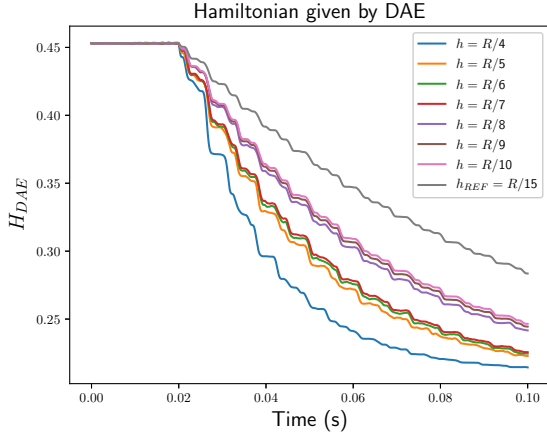


Fig. 4. Hamiltonian trend based on system (19).

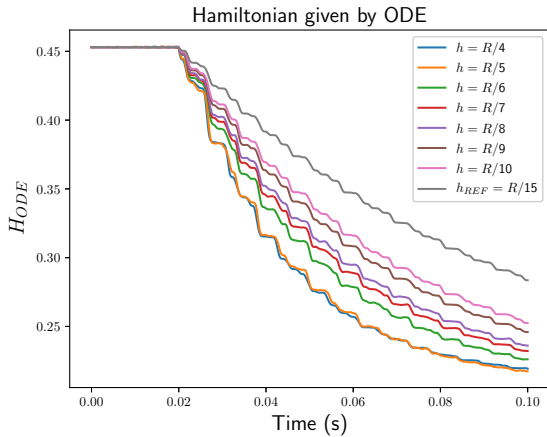


Fig. 5. Hamiltonian trend based on system (28).

Given the physical parameters provided in Tab. 1, the numerical values of the energy contribution are readily found

$$H_v^0 = 0.453[J], \quad H_{vx}^0 = 0.204[J], \quad H_{vr}^0 = 0.249[J].$$

The total energy obtained with increasingly finer mesh is shown in Figs. 4, 5 for the DAE and ODE approach respectively. For coarser meshes, the impedance acts more

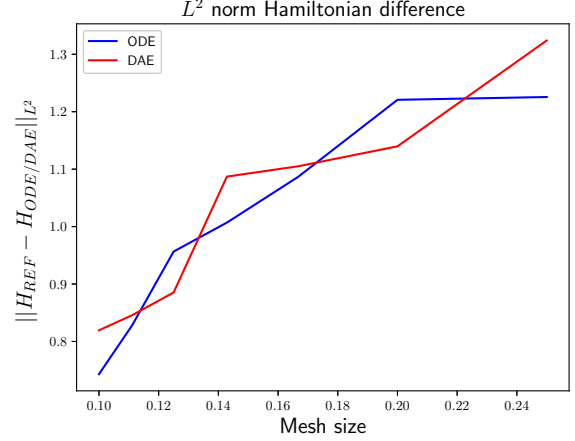


Fig. 6.  $L^2$  error of the Hamiltonian for the two approaches.

$h$ mesh	$\Delta t_{\text{DAE}}[s]$	$\Delta t_{\text{ODE}}[s]$
$R_{\text{ext}}/4$	98.95	124.43
$R_{\text{ext}}/5$	415.99	255.54
$R_{\text{ext}}/6$	798.24	893.63
$R_{\text{ext}}/7$	1408.76	1120.69
$R_{\text{ext}}/8$	3054.78	2271.28
$R_{\text{ext}}/9$	6929.24	5792.89
$R_{\text{ext}}/10$	12648.15	8835.09

Table 2. Elapsed simulation time.

rapidly and the total energy almost reaches the asymptotic value  $H_{vx}(0)$  at  $t_{\text{fin}}$ . For finer meshes the time needed to dissipate  $H_{vr}(0)$  increases, because of the higher inertia. In order to demonstrate the consistency of the two proposed approach the following measure is adopted

$$\varepsilon_{\text{ODE}} = \|H_{\text{REF}} - H_{\text{ODE}}\|_{L^2}, \quad \varepsilon_{\text{DAE}} = \|H_{\text{REF}} - H_{\text{DAE}}\|_{L^2}.$$

Both methods converges monotonically to the reference solution, as illustrated in Fig. 6. The faster convergence of one method on the other cannot be established. Anyway each methodology possesses advantages and drawbacks. The DAE approach (19) guarantees the overall continuity of the variables and does not require the construction two compatibles meshes. The ODE approach (28) requires the construction of two separate mesh and the selection of an appropriate interface boundary  $\Gamma_{\text{int}}$ . This may lead to deformed mesh element and hence less accurate solutions. Furthermore, it does not guarantee the continuity of the fields at the interface. For what concerns the computational cost, in Tab. 2 the simulation time required by each solver is shown. The ODE approach is less time consuming for mesh size sufficiently small. It is important to remark that if the problem is already differential-algebraic Serhani et al. [2019a,b] the domain decomposition technique loses its advantages as the final system will anyway be differential algebraic.

## 6. CONCLUSIONS AND FURTHER WORK

In this work a vibroacoustic application with non-uniform boundary inputs has been addressed. Two different methodologies capable of considering different causalities have been illustrated and compared. Future developments include the employment of theses techniques to more complicated models arising from structural and fluid mechan-



ics. Another valuable contribution would be to reformulate this work in terms of differential forms. This would provide a coordinate free representation and a natural generalization to more complex geometries. A numerical analysis of the optimal choice for the underlying finite elements is still to be done. The introduction of Lagrange multiplier requires the verification of the inf-sup condition. Another interesting topic would be the application of the domain decomposition technique to parallelize simulations of large-scale models.

## REFERENCES

- C. Beattie, V. Mehrmann, H. Xu, and H. Zwart. Linear port-Hamiltonian descriptor systems. *Mathematics of Control, Signals, and Systems*, 30(4):17, 2018.
- F. L. Cardoso-Ribeiro, D. Matignon, and L. Lefèvre. A partitioned finite element method for power-preserving discretization of open systems of conservation laws. *arXiv preprint arXiv:1906.05965*, 2019.
- V. Duindam, A. Macchelli, S. Stramigioli, and H. Bruyninckx. *Modeling and Control of Complex Physical Systems*. Springer Verlag, 2009.
- G. Gatica. *A Simple Introduction to the Mixed Finite Element Method. Theory and Applications*. Springer International Publishing, 01 2014. doi: 10.1007/978-3-319-03695-3.
- P. Grisvard. *Elliptic Problems in Nonsmooth Domains*. Society for Industrial and Applied Mathematics, 2011. doi: 10.1137/1.9781611972030. URL <https://epubs.siam.org/doi/abs/10.1137/1.9781611972030>.
- B. Jacob and H. Zwart. *Linear Port-Hamiltonian Systems on Infinite-dimensional Spaces*. Number 223 in Operator Theory: Advances and Applications. Springer Verlag, Germany, 2012. doi: 10.1007/978-3-0348-0399-1.
- P. Kotyczka. Finite volume structure-preserving discretization of 1d distributed-parameter port-Hamiltonian systems. *IFAC-PapersOnLine*, 49(8):298 – 303, 2016. doi: 10.1016/j.ifacol.2016.07.457. 2nd IFAC Workshop on Control of Systems Governed by Partial Differential Equations CPDE 2016.
- R. Moulla, L. Lefèvre, and B. Maschke. Pseudo-spectral methods for the spatial symplectic reduction of open systems of conservation laws. *Journal of Computational Physics*, 231(4):1272–1292, 2012.
- F. Rathgeber, D.A. Ham, L. Mitchell, M. Lange, F. Luporini, A. T.T. McRae, G.T. Bercea, G. R. Markall, and P.H.J. Kelly. Firedrake: automating the finite element method by composing abstractions. *ACM Transactions on Mathematical Software (TOMS)*, 43(3):24, 2017.
- A. Serhani, D. Matignon, and G. Haine. Anisotropic heterogeneous  $n$ -d heat equation with boundary control and observation: I. Modeling as port-Hamiltonian system. *3rd IFAC workshop on Thermodynamical Foundation of Mathematical Systems Theory (TFMST)*, 2019a.
- A. Serhani, D. Matignon, and G. Haine. Anisotropic heterogeneous  $n$ -d heat equation with boundary control and observation: II. Structure-preserving discretization. *3rd IFAC workshop on Thermodynamical Foundation of Mathematical Systems Theory (TFMST)*, 2019b.
- V. Trenchant, H. Ramirez, Y. Le Gorrec, and P. Kotyczka. Finite differences on staggered grids preserving the port-Hamiltonian structure with application to an acoustic duct. *Journal of Computational Physics*, 373, 06 2018. doi: 10.1016/j.jcp.2018.06.051.
- A.J. van der Schaft and B. Maschke. Hamiltonian formulation of distributed-parameter systems with boundary energy flow. *Journal of Geometry and Physics*, 42(1): 166 – 194, 2002. ISSN 0393-0440. doi: [https://doi.org/10.1016/S0393-0440\(01\)00083-3](https://doi.org/10.1016/S0393-0440(01)00083-3).